ROYAL SOCIETY
OF **CHEMISTRY**

PAPER
Sajal K. Ghosh *et al.*
Nanostructured antimicrobial ZnO surfaces coated with an
imidazolium-based ionic liquid

Check for updates

Nanostructured antimicrobial ZnO surfaces coated with an imidazolium-based ionic liquid

Ajit Seth, Meet Raval, Bishwajit Mandal, Prashant Hitaishi, Priya Mandal,† Samarendra P. Singh and Sajal K. Ghosh ⬡ *

The global COVID-19 pandemic and widespread concerns about antimicrobial resistance (AMR) have intensified research efforts towards the development of innovative methods and technologies to suppress the spread of infectious pathogens facilitated by high touch surfaces. Thus, surfaces and coatings capable of inhibiting bacterial growth and preventing biofilm formation are being comprehensively explored in healthcare sectors to mitigate the spread of infectious pathogens. With the emergence of resistant strains of bacteria, due to over usage of conventional antibiotics, it becomes essential to develop a new class of materials with higher antibacterial efficiency. In the present study, the various morphologies of zinc oxide (ZnO) nanostructures have been exploited as efficient antimicrobial surfaces. This work aims to enhance the bactericidal properties of ZnO nanostructured surfaces by tuning their wettability and surface chemistry. Silicon substrates decorated with ZnO structures such as flowers, needles, and fibers are characterized by scanning electron microscopy (SEM) and atomic force microscopy (AFM). These surfaces are further spin-coated with an ionic liquid 1-decyl-3-methylimidazolium tetrafluoroborate (DMIM-BF4), which causes a drastic impairment of bacterial cell viability on the surfaces. This bactericidal activity has been compared with that of a well-known low surface energy material 1*H*,1*H*,2*H*,2*H*-perfluorooctyl-trichloroethoxysilane (FOTES) by performing spot assay and colony-forming unit (CFU) analysis. The ionic liquids, commonly known as green solvents, are found to be emerging coating materials to develop advanced antimicrobial surfaces.

1. Introduction

Tremendous efforts have long been made to create hierarchical and multifunctional surfaces as a result of the profusion of naturally occurring nanostructured surfaces.[1] Nanotubes, quantum dots, nanoneedles, and nanoflowers have been exceptional in achieving the desired applications.[2] With the advancements in the field of nanotechnology, researchers have been able to explore the utilization of nanomaterials as antimicrobial agents against many pathogens, such as bacteria and viruses.[3] However, in the recent past, the emergence and dramatic increase of pathogenic strains that eventually develop resistance to many antibiotics have been observed.[4]

To address these issues, antibacterial metal oxide nanomaterials are being comprehensively explored because of their stability and negligible toxicity to humans.[5] Among them, ZnO based nanomaterials, "generally recognized as safe" (GRAS)

materials for humans by the US Food and Drug Administration (21CFR182.8991),[6] have been reported to show inherent antibacterial activity towards both Gram-positive and Gram-negative bacteria.[7] Researchers have already reported that the size and morphology of ZnO nanostructures play a crucial role in controlling their antibacterial properties.[8] However, the quantitative analysis of these properties with the change in the morphology of the nanostructures is an area that still requires attention. In a recent paper Tripathy *et al.* reported simple solution-phase fabrication of multifunctional ZnO urchins using zinc nitrate hexahydrate and potassium hydroxide on different substrates.[9] The exact growth mechanism by which ZnO nuclei aggregate to form ZnO nanostructures is best highlighted by Maiti *et al.*, indicating that $Zn(OH)_4^{2-}$, being the main growth precursor, nucleates into zinc oxide nuclei after reaching a critical concentration in the solution mix.[10]

Multiple modifications of metal oxide nanostructures are being carried out to extend their applications in industrial sectors.[11] Coating these nanostructured metal oxide surfaces with particular materials has also been reported to enhance their bactericidal properties.[12–14] One such strategy involves fabrication of superhydrophobic surfaces (water contact angle (CA) > 150°) using a low-energy material like FOTES, which

Department of Physics, School of Natural Sciences, Shiv Nadar Institution of Eminence, NH 91, Tehsil Dadri, G. B. Nagar, Uttar Pradesh 201314, India. E-mail: sajal.ghosh@snu.edu.in

† Present address: 1 Nanoengineered Systems Laboratory, UCL Mechanical Engineering, University College London, London WC1E7JE, UK.

eventually reduces the bacterial growth/attachment on the surfaces.[15] This modification leading to an extensive increase in the hydrophobicity of the surfaces intensifies their applicability[16–21] due to the newly attained anti-corrosion,[22] anti-icing,[23] and self-cleaning properties.[24] However, there is a huge need to look for alternative materials that would be even more lethal to bacteria but environmentally safe.

In the last decade, there has been an enormous amount of investigation on room-temperature ionic liquids (ILs). These ILs are a relatively new class of organic electrolytes composed of an organic cation and an organic or inorganic anion. Owing to their high thermal stability and high thermal and ionic conductivities, these molecules have found use in several other applications[25] such as liquid–liquid separation and designing fuel cells.[26,27] Likewise, due to their low volatility and non-flammability, ILs have also been used as environmentally friendly solvents in many chemical reactions as substitutes for traditional organic solvents.[28–33] They are designated as green solvents because they do not pollute air and can be easily recovered and recycled. Although they may not be toxic to human cells, recent studies have shown the toxicity of these ILs towards microorganisms.[34,35] Early investigation carried out by Pernak et al. showed a trend of increasing antimicrobial toxicity with an increase in the C-1 alkyl chain length in imidazolium-based ionic liquids.[36] It is further shown that varying the anion had a minimal effect on the toxicity of imidazolium-based ILs, indicating that toxicity is largely driven by the alkyl chain length and hydrophobicity of the cation.[37]

Generally, the ILs have been used in solution form to study their antimicrobial properties. However, the applicability of ILs as coating materials, either in their pristine form or as a part of a composite material, has also been explored. These coatings eventually help to render surfaces with excellent antibacterial, antibiofouling and anticorrosive properties.[38–40] For instance, Bains et al. developed ionic liquid (IL)-functionalized multi-walled carbon nanotubes for hydrophobic and antibacterial coatings.[38] They showed that coating the polyvinyl chloride substrates with the synthesized ionic liquid–carbon nanotube composite eventually turned them into robust self-sterilizing surfaces. Similarly, Misra et al. fabricated thin films of polyoxometalate-based ionic liquids using brush-coating on the surface of stones to protect them from acid corrosion and also enhance their biocidal properties.[39] Imidazolium based ionic liquid coatings have also shown excellent potential as emerging antibacterial coatings.[41–43] Correspondingly, higher toxicity of imidazolium based ionic liquid coatings towards bacterial cells than mammalian cells has been confirmed by Gindir et al.[41]

Considering the toxic nature of ILs towards bacteria, integration of ILs with ZnO nanostructures could possibly help in further enhancing the antimicrobial activity of such structured surfaces. In a recent paper presented by Xiaohan Zhang, spin coating of an IL on a ZnO surface has been demonstrated.[44] In the present study, various ZnO nanostructures with various shapes have been synthesized on a silicon substrate and characterized by scanning electron microscopy (SEM) and

atomic force microscopy (AFM). These structures are then coated with an imidazolium-based IL to figure out the modifications in the wetting and bactericidal properties of the surfaces. The development of ILs as coating materials for nanostructured surfaces turns out to be useful in enhancing their antibacterial properties. The results have also been compared with a well-known superhydrophobic coating material FOTES.

2. Materials and methods

2.1 Materials

Zinc acetate dihydrate $[Zn(CH_3COO)_2 \cdot 2H_2O]$, zinc nitrate hexahydrate $[Zn(NO_3)_2 \cdot 6H_2O]$, 2-methoxy ethanol $[C_3H_8O_2]$, ethanolamine $[C_2H_7NO]$, potassium hydroxide (KOH), $1H,1H,2H,2H$-perfluorooctyltriethoxysilane (FOTES) and 1-decyl-3-methylimidazolium tetrafluoroborate (DMIMBF$_4$) were purchased from Sigma-Aldrich (now Merck, USA) and used without further purification. The Luria-Bertani (LB) broth and LB agar medium for the bacterial growth study were obtained from Hi-Media (Mumbai, India). The spectroscopic grade methanol and ethanol were purchased from Thermo Fisher Scientific (USA). De-ionized (DI) (Milli-Q, Millipore) water with a resistivity of ~ 18 MΩ cm and a pH of ~ 7.0 has been used throughout the experiment.

2.2 Developing structured substrates

2.2.1 Substrate preparation and cleaning. Silicon substrates of size 1.5×1 cm^2 were cut from silicon wafer (n-type, ⟨100⟩, 500 μm thick, WaferPro) using a diamond cutter. All the substrates were cleaned ultrasonically using 15 minute cycles of methanol and DI water, respectively. After completion of ultrasonication, the samples were dried carefully using N$_2$ flow. Then the substrates were kept in a UV-ozone chamber at 50 °C for 30 minutes with 10 minutes of hold time to make them hydrophilic by evaporating all the organic impurities from the surfaces.

2.2.2 Growth of ZnO nanostructures. In the first step, the seeding procedure was performed in order to create nucleation sites for the growth of ZnO nanostructures on the Si substrate. The cleaned substrates were seeded with an ethanol solution of zinc acetate dihydrate with a concentration of ~ 1 mg mL^{-1}. The solution was stirred for 15 minutes at 300 rpm to properly dissolve the solute in the solvent. Then, 15 μL of this solution was dropped on top of the substrate and dried gently using a N$_2$ purging instrument with an opening comparable to the sample width to ensure its slow evaporation. This coating procedure is repeated five times, each time increasing the volume of the solution pipetted on the substrate by 1 μL to form a uniform seed layer. Later, the seeded substrates were heated at 300 °C in an oven (microprocessor controlled oven, Metrex Scientific Instruments (P) Ltd., New Delhi) and annealed for 60 minutes. In the second step, the aqueous solution of zinc nitrate hexahydrate (~ 30 mg mL^{-1}) was added dropwise to an aqueous potassium hydroxide solution (~ 50 mg mL^{-1}) under

constant stirring at 500 rpm. The resulting mixture turned turbid due to the nucleation reaction of $Zn(OH)_4^{2-}$ to form ZnO nucleates. Then, this solution was carefully poured into the glass Petri dish containing the annealed silicon substrates. The Petri dishes were sealed with paraffin films and kept at 25 °C for 12 hours to obtain nanoflower structures. For obtaining nanoneedle structures, the samples were kept in the solution at 100 °C for 24 hours. After synthesis the samples are rinsed with DI water, dried under N_2 flow, and kept in a desiccator at controlled humidity (RH ∼ 20%).

For growing nanofibers, a different approach was adopted. Here, the ZnO precursor solution was prepared by mixing zinc acetate dihydrate (106 mg), 2-methoxy ethanol (980 μL), and ethanolamine (20 μL), and then, the mixture was stirred at 55 °C for 12 hours at 350 rpm. After being treated with UV-ozone for 20 minutes at 100 °C, the cleaned silicon substrates were coated with ZnO precursor solution by spin coating at 2000 rpm for 60 s and then annealed at 150 °C for 15 minutes.[45,46] Note that, for each fabricated nanostructured surface, the existence of ZnO on the Si substrate was established by elemental mapping using Energy Dispersive X-ray Analysis (EDAX) (data not shown).

2.3 Coating synthesized substrates

2.3.1 FOTES coating. The substrates were coated with FOTES by the physical vapour deposition (PVD) process. In brief, the substrates were placed on the base of a desiccator, and 150 μL of FOTES was taken in a glass vial and placed on the base of the desiccator. The desiccator was sealed using a vacuum pump to a pressure of 0.08 bar and kept in an oven at 150 °C for 1.5 hours. To coat more than four samples at once, the amount of FOTES in the desiccator was increased by placing another glass vial containing 150 μL of FOTES. After bringing it down to room temperature, the vacuum was released and the FOTES coated substrates were cleaned ultrasonically with DI water. After drying with a stream of N_2 flow, the substrates were then kept at 50 °C at least a day before further use.

2.3.2 Ionic liquid (IL) coating. The IL $DMIMBF_4$ was spin-coated on silicon and nanostructured substrates. The flat silicon substrate without any ZnO nanostructure was taken as the control to compare the effect of the nanostructure. The effect of the coated nanostructure was compared with that of the nanostructured surface without any coating. 0.3 wt% of this IL added in methanol was ultrasonicated for 5 minutes to dissolve completely. 50 μL of this solution was pipetted on top of the substrate and spin-coated (spinNXG-P1A, Apexicindia) at 4000 rpm for 1 minute. Finally, the samples were annealed in an oven at 100 °C for 30 minutes.

Note that the thickness of the coating layer of FOTES and IL is low compared to the dimensions of the nanostructures on the Si substrate, and therefore, the underlying ZnO morphology is expected to remain intact after the coating.

2.4 Characterizing surface activity

2.4.1 Surface wettability. Wettability of the control and treated substrates was quantified by measuring the water contact angles (APEX, ACAM Series). The contact angles were measured using a sessile drop method with 5 μL of de-ionized (DI) water at a dosing rate of 0.32 mL min^{-1}. The contact angles were calculated using the ImageJ software. For each case, at least three measurements were taken at different regions of a particular surface to find a statistically averaged value. All these measurements were performed at 24 ± 2 °C and at an RH of 50%.

2.4.2 Antibacterial activity. Luria-Bertani (LB) broth, composed of casein enzymic hydrolysate, yeast extract, sodium chloride, and agar, is a commonly used nutritionally rich medium for the bacteria culture process. 40 gm of this mixture was dissolved in 1000 mL of DI water and autoclaved at 120 °C for 20 minutes to sterilize the medium. After cooling to a temperature of 60 °C, it was poured into sterile Petri plates. Once solidified, it was wrapped with parafilm and stored at 4 °C for further use. For sufficient growth of bacteria, the required vitamin B complexes are supplied by the yeast extract, while the casein enzymic hydrolysate provides peptides and peptones. Sodium chloride helps in membrane transport and maintains the osmotic equilibrium of the medium.

For the primary culture, the glycerol stock solution of Gram-negative bacteria, *E. coli* (dh5, alpha),[47,48] was taken and grown overnight at 37 °C in the LB broth medium with gentle shaking at 200 rpm following the protocol reported elsewhere.[49–51] 1 mL of this culture was then added to fresh LB broth to reach a final optical density (OD600) of 0.2. A drop of 80 μL of this solution was placed on the surface of structured substrates and incubated for a period of 4 hours. The cells were allowed to grow on the polished Si, ZnO nanofibers, ZnO nanoneedles, and ZnO nanoflowers surfaces at 37 °C. Then, the cells were pipetted out from the respective surfaces into 0.9% saline solution and stored in a sterile Eppendorf tube. For spot assay, 5 μL of this solution of different dilution series was spotted on MacConkey agar plates (Hi-Media, Mumbai), and the plates were kept overnight at 37 °C. The observed number of colonies were counted manually. For calculating the colony-forming unit (CFU), a 100 μL solution of a particular dilution was taken in a sterile LB agar plate and uniformly spread with a spreader. It was left for a few minutes at room temperature to dry and, thereafter, stored at 37 °C for 12 hours. CFU per mL is calculated using the following relation,

$$\text{CFU per mL} = \frac{\text{No of colonies} \times \text{dilution factor}}{\text{volume of culture spread on agar plate (in mL)}} \quad (1)$$

3. Results and discussion

3.1. Surface morphology

The wetting properties and initial attachment of bacteria cells on a nanostructured surface undoubtedly depend on its morphology.[52] In order to study this dependence, three types of ZnO nanostructured surfaces are synthesized, namely nanoflowers, nanoneedles, and nanofibers. Fig. 1 shows the
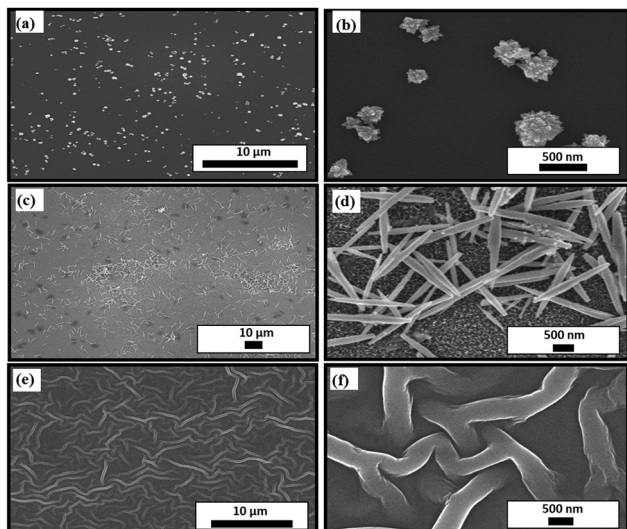
Fig. 1 Scanning electron microscopy (SEM) images of (a) ZnO nano-flowers, (c) ZnO nanoneedles, and (e) ZnO nanofibers synthesized on a silicon substrate with their enlarged views in (b), (d) and (f) respectively.

scanning electron microscopy (SEM) images of all the different nanostructures formed on a silicon substrate. Their dependence on the parameters of their synthesis processes, as described in Section 2, eventually illustrates the difference in their morphologies. The variation in surface coverage of different nanostructured surfaces can be visualized in Fig. 1. While the nanoflowers show the minimum surface coverage (Fig. 1(a)), there is a maximum density of structures in the case of nanofibers (Fig. 1(e)). This can indeed lead to distinct

bactericidal properties of these surfaces. The fibers seem to be interweaved, lying on the substrate. The average basal lengths, as seen in the corresponding zoomed-in images of the nanoflowers (Fig. 1(b)) and nanoneedles (Fig. 1(d)), are around 288 ± 120 nm and 1000 ± 200 nm, respectively. This difference in the morphologies of these structures can be attributed to the differentiated response of a seeded silicon substrate to the synthesis parameters. The variation in the exposure time and temperature of a seeded silicon substrate to the muddled solution containing $Zn(OH)_4^{2-}$ ions affects the nucleation process and further growth mechanism.[53]

The complete surface morphology represented by the three-dimensional spatial structures can be observed in Fig. 2, which shows the atomic force microscopy (AFM) images. It can be inferred from the images that the growth of nanostructures on a smooth silicon surface makes it uneven and hence should increase the roughness of the surface depending on the density of structures. This can be verified from the surface roughness data in Table 1. There is a gradual increase in the average roughness and root mean square (RMS) roughness of the samples with a trend of silicon < flowers < needles < nanofibers. This trend in the roughness values is directly related to the coverage of the substrate by nanostructures. This varying coverage of the substrates by the nanostructures can also be verified from their corresponding height profiles, as shown in the inset of Fig. 2.

3.2 Surface wettability

The measurement of the water contact angle for a nanostructured surface quantifies its wetting behaviour. The values of
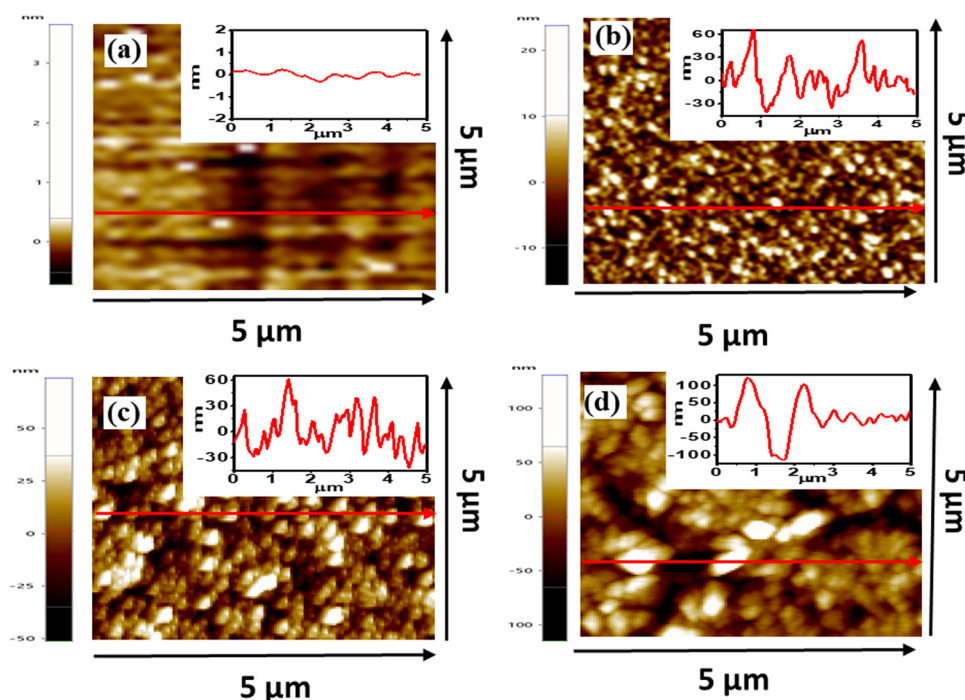

Fig. 2 Atomic force microscopy (AFM) images of (a) silicon, (b) ZnO nano-flowers, (c) ZnO nanoneedles, and (d) ZnO nanofibers. Inset shows the height profile of respective line drawn in an image.

Table 1 The topographical parameters of surfaces: average roughness and root mean square roughness of all the nanostructured surfaces as obtained from their AFM images

Samples	Average roughness (nm)	RMS roughness (nm)
Silicon	0.15	0.23
ZnO nanoflowers	3.96	5.04
ZnO nanoneedles	14.46	18.38
ZnO nanofibers	25.25	33.06

the contact angle (θ) depend on the physical roughness and the chemical nature of the surface.[54] Depending on the value of θ, solid surfaces are categorized into four types: (i) super hydrophilic ($0° < \theta < 10°$), (ii) hydrophilic ($10° < \theta < 90°$), (iii) hydrophobic ($90° < \theta < 150°$) and (iv) superhydrophobic ($150° < \theta < 180°$). For a perfectly smooth surface, the obtained value of θ is generally governed by Young's equation[55] given by,

$$\cos\theta = \frac{\gamma_{SV} - \gamma_{SL}}{\gamma_{LV}} \qquad (2)$$

where γ_{SV}, γ_{SL}, and γ_{LV} are the interfacial energies at solid–vapor, solid–liquid, and liquid–vapor interfaces, respectively. On the other hand, for a heterogeneous or a nanostructured surface, this contact angle value is characterized by the Wenzel[56] and Cassie–Baxter[57] models. These models suggest that values of the contact angle obtained for the corresponding nanostructured surfaces are a combination of their respective surface roughness and the area covered by the nanostructures on a substrate.

In order to modify their wetting properties and eventually their antibacterial efficiency, the surfaces have been coated with a low surface energy molecule 1H,1H,2H,2H-perfluorooctyltriethoxysilane (FOTES) with chemical structure $C_{16}H_{19}F_{17}O_3Si$. Fig. 3(a) shows the optical images of a 5 μL sessile drop of DI water on the uncoated and coated surfaces. In

Fig. 3(b), the corresponding values of contact angles of uncoated, DMIMBF$_4$ coated, and FOTES coated substrates, quantified from multiple measurements, are given in bar diagrams. In this case, the control sample is a polished bare silicon substrate with a contact angle (θ) of $69.7 \pm 1.2°$ ($\theta < 90°$), indicating the inherent hydrophilic nature of the surface. The corresponding values of the contact angle obtained for the uncoated nanoflowers, nanoneedles, and the nanofibers are $55.2 \pm 2.9°$, $44 \pm 2°$, and $18.6 \pm 3°$, respectively. The decrease in the contact angle values or the enhanced hydrophilicity of the surfaces is in accordance with the nature of metal oxide coatings due to the existence of hydroxyl groups, metal cations, and oxygen anions.[58] Particularly, in the case of ZnO nanofibers the uniform dense coverage provides a sea of oxygen atoms for the incoming water droplet to spread out *via* hydrogen bonding, leading to the smallest contact angle. For nanoneedles and nanoflowers, the varying morphology due to synthesis parameters leads to different contact angle values. The sample with nanoneedles is more hydrophilic than the sample with nanoflowers because of the higher density of nanostructures in the former case. This yet again supports the characteristics of a metal oxide surface. This observation also shows the fact that a hydrophilic surface becomes more hydrophilic upon increasing the surface roughness.[59] As listed in Table 1, the increased roughness of the surface follows the trend, nanofibers > nanoneedles > nanoflowers > silicon, which is opposite to the measured contact angles of the surfaces, nanofibers < nanoneedles < nanoflowers < silicon.

In the case of FOTES-coated samples for all the different types of structures, the de-wetting properties of the surfaces are readily enhanced, as observed by a considerable increase in the contact angle values. The silane head part of the FOTES molecule gets attached to the metal surface because of an attractive interaction. In contrast, the tail part comprised of a
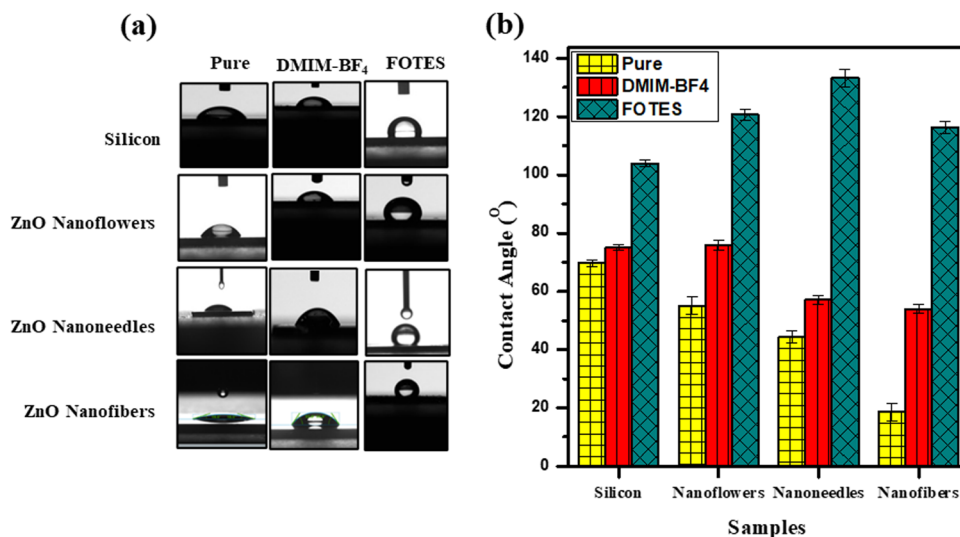

Fig. 3 (a) The optical images of a 5 μL water droplet standing on different samples with various surface morphologies. (b) Variation of the contact angle on silicon and all other nanostructured surfaces with different types of coatings. DMIM-BF$_4$ is an imidazolium based ionic liquid and FOTES is a low energy hydrophobic material. The results of a flat silicon surface are compared with those of the surfaces covered with different nanostructures formed by ZnO.

fluorinated chain hangs in air, which repels water molecules because of its hydrophobic nature. The highest value of contact angle for a FOTES-coated sample is obtained for the nanoneedles, *i.e.*, $133.2 \pm 3°$. The nanoflowers display a contact angle of $120.7 \pm 2°$, while the nanofibers show a contact angle of $116.4 \pm 2°$. Even though the roughness of a nanofiber surface is the maximum, because of excellent surface coverage, it traps lowest quantity of air. On the other hand, with a medium surface coverage and roughness, the nanoneedle surface has much more trapped air causing the water droplet to exhibit the highest contact angle after being coated with FOTES. Similarly, for ionic liquid (DMIMBF$_4$) coated samples, there is an increase in the contact angle values for all the cases compared to the uncoated ones. However, the effect of hydrophobicity is not as strong as the FOTES molecules. This is in line with the difference in their molecular structures as fluorocarbons are more hydrophobic compared to the hydrocarbons.[60] The shorter positively charged imidazolium head group of DMIMBF$_4$ interacts with the nanostructured surface, while the hanging hydrocarbon tail in air is responsible for the increased hydrophobicity.

3.3 Morphological and immersion stability

The modification of the morphological and wetting characteristics of a nanostructured surface is only feasible when the coating does not necessarily damage the structural integrity of the surface. Fig. 4(a) shows the SEM images of nanoneedle samples after being coated with FOTES and DMIMBF$_4$, respectively. These coatings do not modify the morphology of the surfaces as the nanostructures remain unaltered. This further rationalizes the use of the coated surfaces in applications considering only the morphology of the surfaces.

The firmness of the coatings is studied by examining their immersion stability. The process involves immersing the coated samples in water and measuring the contact angles after specific time intervals. The samples are dried thoroughly under N$_2$ flow before measuring the contact angles. Fig. 4(b) shows the immersion stabilities of both the FOTES and DMIMBF$_4$ coated surfaces. Predominantly, one of the purposes of altering the surface properties to obtain a sufficiently hydrophobic surface is to realize its usage in applications involving its immersion in water.[61] Therefore, this test is essential. Even though there is a few degree drop in the contact angle, it can be inferred from Fig. 4(b) that the hydrophobic FOTES-coated surfaces, under submerged conditions, do not lose their de-wetting properties drastically. This is true for all the nanostructured and polished silicon samples, affirming the firmness of the coatings. For the DMIMBF$_4$ coated samples, there is a decrease in the contact angle values for the first immersion cycle of 4 hours. Such a decrease is also observed when the coated sample is immersed in LB broth. This can be attributed to the fact that even though the DMIMBF$_4$ coating increases a surface's hydrophobicity, the samples are, nonetheless, hydrophilic in nature, with contact angles less than 90° for every case. Interestingly, compared to the data from the first cycle, no considerable change in the contact angle is observed for the
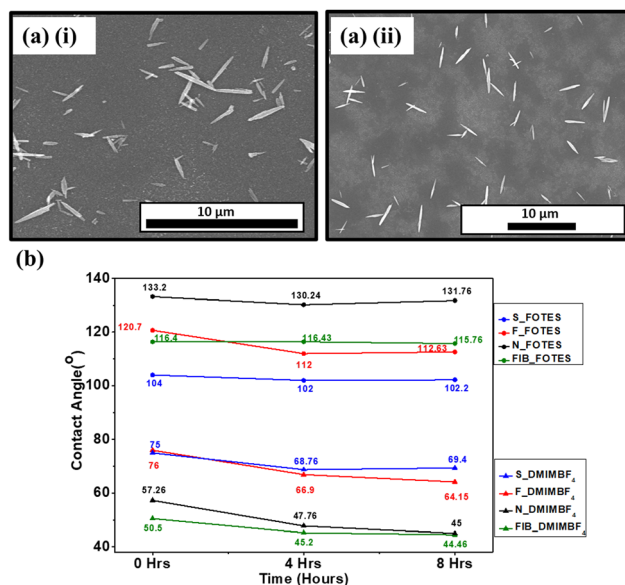

Fig. 4 (a) FESEM images of nanoneedles after coating with (i) FOTES and (ii) DMIMBF$_4$. (b) Water contact angle values of FOTES and DMIM-BF4 coated silicon, ZnO nanoflowers, ZnO nanoneedles, and ZnO nanofibers after 4 hours and 8 hours of immersion in DI water. Here, S_FOTES represents silicon coated with FOTES, similarly S_DMIMBF$_4$: silicon coated with DMIMBF4; F_FOTES: nanoflowers coated with FOTES; F_DMIMBF$_4$: nanoflowers coated with DMIMBF$_4$; N_FOTES: nanoneedles coated with FOTES; N_DMIMBF$_4$:needles coated with DMIMBF$_4$; FIB_FOTES: nanofibers coated with FOTES and FIB_DMIMBF4: nanofibers coated with DMIMBF$_4$.

next immersion cycle of 8 hours. This specifies that the DMIMBF$_4$ coating withstands the immersion stability test and can be efficiently used for applications involving immersion in water.

3.4 Bactericidal efficiency of surfaces

ZnO nanostructures grown on surfaces as well as nanoparticles in powder form have established themselves as materials with highly competent bactericidal properties.[62] With the purpose of targeting the gradual emergence of antimicrobial-resistant bacteria, the current work suggests making strides toward significantly enhancing the antibacterial properties of nanostructured ZnO surfaces. The antibacterial activities of all the DMIMBF$_4$ and FOTES-coated ZnO samples are measured through spot assays and plate counting methods, by observing the viability of Gram-negative bacteria *E. coli*. Fig. 5 shows the spot assays of all the nanostructured surfaces, with bare silicon as the control. It demonstrates a qualitative view of the viability of the bacterial cells on the polished Si, ZnO nanoflowers, ZnO nanoneedles, and ZnO nanofibers for different dilution series. As observed, the unprocessed polished silicon substrates seem to relatively sustain the growth of bacteria. Looking at the 4th and 5th dilution series for all the uncoated samples, it can be inferred that the presence of nanostructures hampers the growth of bacteria compared to a bare silicon substrate. Compared to the nanoneedle sample, sufficient bacterial growth is observed in the nanoflower sample because of their low surface
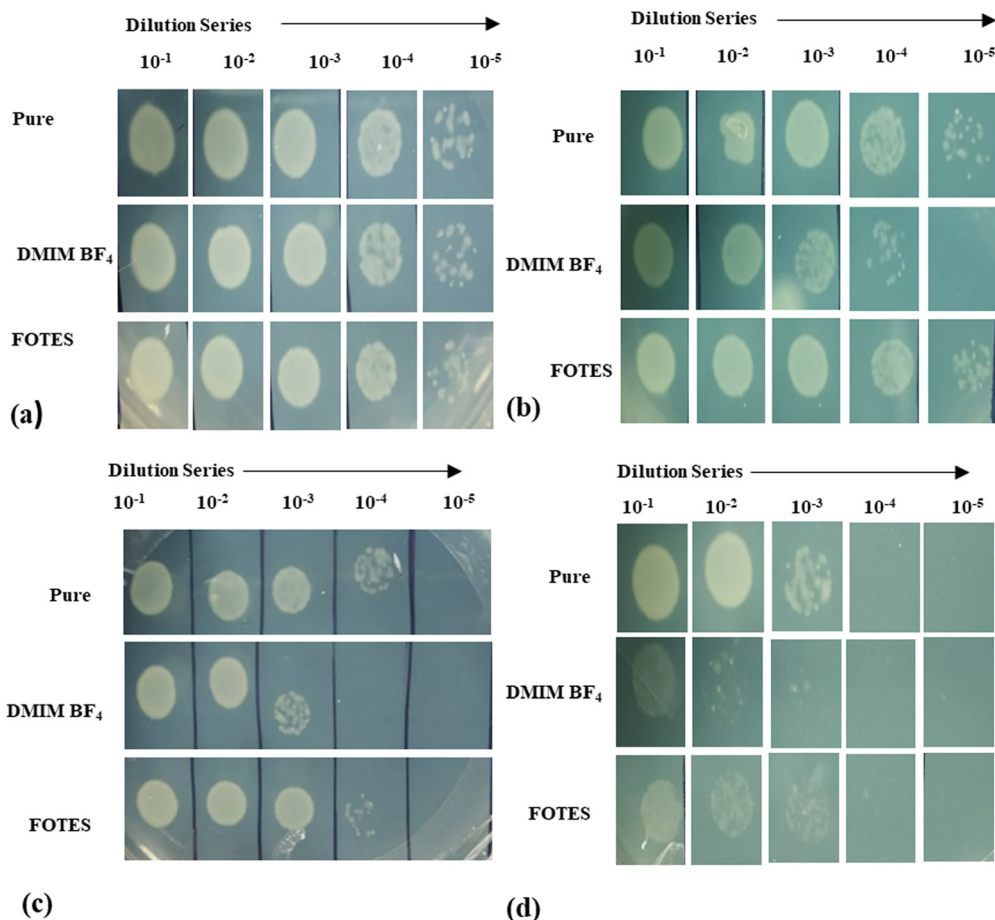
Fig. 5 Spot assay after 4 hours of incubation on (a) silicon, (b) ZnO nanoflowers, (c) ZnO nanoneedles and (d) ZnO nanofibers.

coverage. The nanofiber samples with excellent surface roughness and surface coverage show the highest bactericidal activity. Hence, from these comparisons, it can be found that the ability of the nanostructured surfaces to diminish the bacterial viability can be considered to be solely dependent on their morphology and density.

In the case of coated samples, primarily FOTES-coated surfaces, the bacterial colonies are drastically reduced compared to their uncoated counterparts, as can be seen again for the 4th and 5th dilution series. There is a drastic reduction in the bacterial growth in comparison to the pure silicon control samples. On the other hand, a comparison of even the 2nd and 3rd dilution series of the DMIMBF$_4$ coated samples with their FOTES-coated and pure counterparts shows further reduction in the bacterial colonies. This qualitative analysis performed using the spot assays has also been verified by counting the colony-forming units (CFU per mL). CFU per mL after 4 hours of incubation of bacterial cells on all the different substrates is shown in Fig. 6(a). Fig. 6(b) shows a representative set of pictures demonstrating the number of bacterial colonies (white spots) formed for uncoated and coated ZnO nanofiber samples. It is apparently evident that uniformly dense pure ZnO nanofiber structures are observed to have brilliant bactericidal properties with almost little to negligible bacterial cells

remaining active on the surface. Comparatively the sparsely grown sharp ZnO nanoneedles and nanoflowers cause multiple perforations in the bacterial cell wall due to mechanical rupture. Furthermore, coating the substrates with DMIMBF$_4$ turns out to be most advantageous for tackling the growth of bacterial colonies, as the least value of CFU for all the different nanostructured surfaces is observed for this case.

It is observed that the contact angle values of LB broth containing *E. coli* on the fabricated surfaces are relatively low compared to water (data not shown). However, they follow qualitatively a similar trend as that of water. These lower contact angles ensure that the LB broth is well in contact with the surfaces and, hence, the slow growth of bacteria is indeed induced by the fabricated surfaces and the coatings.

3.5 Ionic liquid as a coating material

There are multiple processes and mechanisms that are involved in controlling the growth of bacteria on a surface. The researchers are focussing on the following major mechanisms to develop better bactericidal surfaces:

(1) The antibacterial activity is a consequence of the generation of reactive oxygen species (ROS). These ROS include hydrogen peroxide (H_2O_2), superoxide anions ($O_2^{\bullet-}$), and hydroxyl radicals ($OH^{\bullet}$), which hinder bacterial metabolism
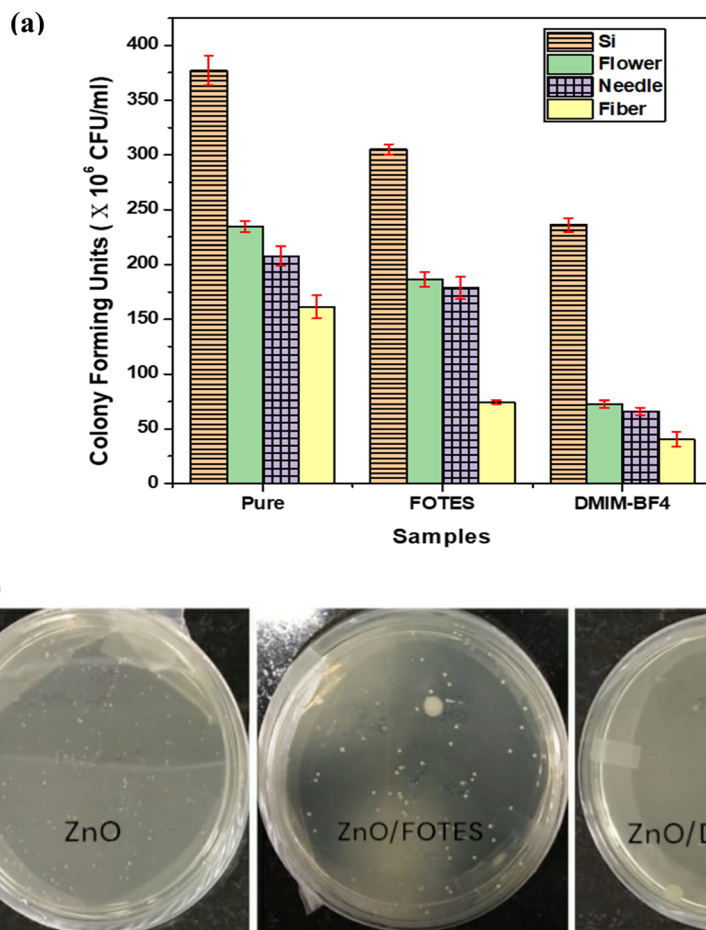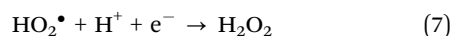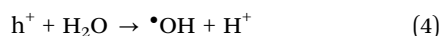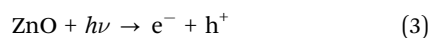
Fig. 6 (a) The number of colony Forming Units (CFUs) after 4 hours of incubation on silicon, ZnO nanoflowers, ZnO nanoneedles and ZnO nanofibers. (b) Bacterial colony (while spots) formed on uncoated, FOTES-coated and DMIM-BF4 coated ZnO nanofiber samples respectively. The ionic liquid DMIM-BF4 coated sample shows the least number of colonies on the surface.

and interrupt different functionalities of a cell, leading to cell death.[63–71] The formation of ROS leads to the gradual disintegration of the cellular membrane because of lipid peroxidation and distresses the functionality of mitochondria.[72] ZnO is reported to be one of the active metal oxides showing the ROS mechanism for diminishing the bacterial growth on a surface.[62] Researchers have shown the generation of ROS on ZnO nanostructured surfaces under both UV and visible light irradiation.[67] The generation of ROS is governed by the following equations:[67]

$$ZnO + h\nu \rightarrow e^- + h^+ \tag{3}$$

$$h^+ + H_2O \rightarrow {}^\bullet OH + H^+ \tag{4}$$

$$e^- + O_2 \rightarrow {}^\bullet O_2 \tag{5}$$

$$O_2 + H^+ \rightarrow HO_2{}^\bullet \tag{6}$$

$$HO_2{}^\bullet + H^+ + e^- \rightarrow H_2O_2 \tag{7}$$

While the generated hydroxyl and superoxide radicals interact with the cellular membrane leading to membrane disruption,[6] the hydrogen peroxide molecules conveniently penetrate the

bacterial cell causing extensive damage to the internal components eventually leading to cell death.[70]

(2) The ROS mechanism demands a higher contact area of a bacterium with the surface. As the nanostructured surface has a higher surface-to-volume ratio, it primarily interferes with the cellular mechanism to a high extent following the ROS mechanism. Secondarily, compared to a smooth surface, the advanced morphology of nanostructures leads to the mechanical rupture of bacterial cells.[63–67,73–75] A nanostructure on a surface is multiple orders of magnitude smaller with respect to the size of a bacterium. Therefore, the physical piecing and penetration of the structure into a cell is obvious, which has been verified by SEM images.[15,49,50,76] This physical rupture is necessarily dependent on the nanostructure's optimum shape and size as observed for the flowers, needles and fibers.

(3) The wettability of a surface developed by coating with various materials controls the interaction of a bacterial cell with it. A superhydrophilic surface can have an attractive interaction with the bacteria, while a superhydrophobic surface repels them. A nanostructured superhydrophilic surface can pull the bacteria leading to cell death because of physical rupture and the surface chemistry.[51] A superhydrophobic surface does not
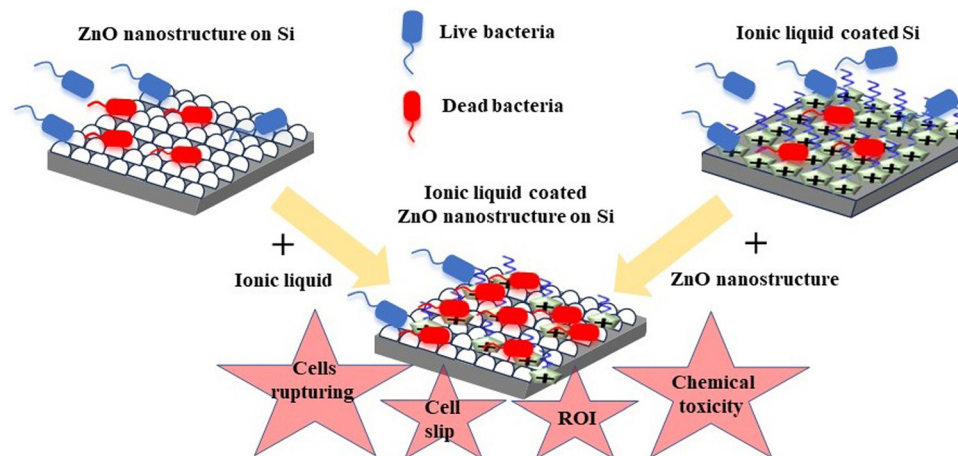
Fig. 7 Schematic illustration of enhanced bactericidal properties of ZnO nanostructured silicon substrates coated with an ionic liquid. ROI denotes reactive oxygen ion.

provide enough surface energy for the bacterial cells to grow and eventually leads to cell slip-off, which can readily be observed in FOTES-coated samples in the present study and the previously reported studies.[51,77]

(4) There are other mechanisms reported in a few studies. A study on ZnO at room temperature has reported that UV irradiation[9] is responsible for reducing bacterial growth. Other studies have also shown that the cell degradation process occurred due to excess zinc resulting in DNA replication disruption and DNA breakage.[78] Also, researchers have shown how disturbance is induced in enzymatic systems and other metabolic processes due to Zn^{2+} ions that are released from ZnO nanoparticles.[79]

Although there are reports on all of these mechanisms, the search for new and highly efficient bactericidal surfaces is ongoing. The novelty of the present study lies in using an environmentally friendly green solvent, ionic liquid, as a coating material and achieving excellent antibacterial activity. Ionic liquids are unique materials with high thermal stability and low vapor pressure.[80] As a consequence, they do not pollute air and have a remarkable recovery rate from marine water bodies.[81] Interestingly, the antibacterial nature of imidazolium ionic liquids has been observed for quite a long time.[82] Furthermore, although they control the growth of bacteria or tumor cells, they are safe for healthy human cells.[83] There have been numerous studies suggesting the increase in the toxicity of these molecules with an increase in their hydrophobicity because of larger alkyl chains. Studies have suggested bacterial cell death due to extensive membrane disruption.[82,84,85] The present study uses these extraordinary bactericidal properties of ionic liquids by coating $DMIMBF_4$ on inherently antibacterial ZnO nanostructured surfaces. On top of the ROS mechanism and nanostructure effects, the native chemical nature of disintegrating the self-assembly of the bacterial membrane by the ionic liquid produces a composite surface with an aim to tackle the antibiotic-resistant bacteria. A schematic representation of these collective effects is shown in Fig. 7.

Although this work suggests the ionic liquid to be an exciting coating material, more systematic and extensive studies are required. A point would be to find a better mechanism to enhance the stability of the coating on the surface under harsh conditions. Furthermore, various other metallic surfaces, such as aluminium, copper and steel, which have extensive industrial applications, have to be investigated. One has to also explore the chain lengths and combination of cations/anions of different ionic liquids to find out suitable molecules for a specific purpose.

4. Conclusions

This work discusses the development of bactericidal ZnO nanostructures and their dependence on their various surface morphologies. The study shows how different parameters such as shapes and roughness of the nanostructures on the surface control their bactericidal properties. This is verified by characterization techniques, including SEM, AFM, and water contact angle analysis. The ZnO nanostructures are further coated with FOTES and an imidazolium-based ionic liquid $DMIMBF_4$ to observe the change in their antibacterial activity. Both spot assays and colony-forming unit (CFU) analysis confirm further increased bacterial cell death in the presence of the coatings. The nanostructured surfaces with the $DMIMBF_4$ coating are found to be the most bacteria-repelling surfaces compared to their FOTES-coated counterpart. These ionic liquid coated ZnO surfaces could be used in the future as advanced bactericidal surfaces for industrial applications.

Conflicts of interest

The authors declare that they have no known competing financial interests or personal relationships that could have appeared to influence the work reported in this paper.

Acknowledgements

References

1 A. Sirelkhatim, S. Mahmud, A. Seeni, N. H. M. Kaus, L. C. Ann, S. K. M. Bakhori, H. Hasan and D. Mohamad, Review on zinc oxide nanoparticles: antibacterial activity and toxicity mechanism, *Nano-Micro Lett.*, 2015, **7**, 219–242.

2 D. Chen, Q. Wang, R. Wang and G. Shen, Ternary oxide nanostructured materials for supercapacitors: a review, *J. Mater. Chem. A*, 2015, **3**, 10158–10173.

3 L. Wang, C. Hu and L. Shao, The antimicrobial activity of nanoparticles: present situation and prospects for the future, *Int. J. Nanomed.*, 2017, **12**, 1227–1249.

4 U. Desselberger, Emerging and re-emerging infectious diseases, *J. Infect.*, 2000, **40**, 3–15.

5 S. H. Lee and B.-H. Jun, Silver nanoparticles: synthesis and application for nanomedicine, *Int. J. Mol. Sci.*, 2019, **20**, 865.

6 Y. Xie, Y. He, P. L. Irwin, T. Jin and X. Shi, Antibacterial activity and mechanism of action of zinc oxide nanoparticles against Campylobacter jejuni, *Appl. Environ. Microbiol.*, 2011, **77**, 2325–2331.

7 K. S. Siddiqi and A. Husen, Properties of zinc oxide nanoparticles and their activity against microbes, *Nanoscale Res. Lett.*, 2018, **13**, 1–13.

8 S. Al-Heniti and A. Umar, Structural, optical and field emission properties of urchin-shaped ZnO nanostructures, *J. Nanosci. Nanotechnol.*, 2013, **13**, 86–90.

9 A. Tripathy, P. Wąsik, S. Sreedharan, D. Nandi, O. Bikondoa, B. Su, P. Sen and W. H. Briscoe, Facile fabrication of multifunctional ZnO urchins on surfaces, *Colloids Interfaces*, 2018, **2**, 74.

10 U. N. Maiti, A. Sen, M. K. Mitra and K. K. Chattopadhyay, Simple Solution Phase Synthesis of 3-D Assembly of ZnO Nanoneedles and Its Efficient Field Emission, *J. Nanosci. Nanotechnol.*, 2010, **10**, 4341–4347.

11 X. Zhang, L. Wang and E. Levänen, Superhydrophobic surfaces for the reduction of bacterial adhesion, *RSC Adv.*, 2013, **3**, 12003–12020.

12 A. B. Djurišić, Y. H. Leung, A. M. Ng, X. Y. Xu, P. K. Lee, N. Degger and R. Wu, Toxicity of metal oxide nanoparticles: mechanisms, characterization, and avoiding experimental artefacts, *Small*, 2015, **11**, 26–44.

13 S. M. Dizaj, F. Lotfipour, M. Barzegar-Jalali, M. H. Zarrintan and K. Adibkia, Antimicrobial activity of the metals and metal oxide nanoparticles, *Mater. Sci. Eng., C*, 2014, **44**, 278–284.

14 M. Horie, K. Fujita, H. Kato, S. Endoh, K. Nishio, L. K. Komaba, A. Nakamura, A. Miyauchi, S. Kinugasa and Y. Hagihara, Association of the physical and chemical properties and the cytotoxicity of metal oxidenanoparticles: metal ion release, adsorption ability and specific surface area, *Metallomics*, 2012, **4**, 350–360.

15 P. Mandal, J. Ivvala, H. S. Arora, H. S. Grewal and S. K. Ghosh, Structured aluminium surfaces with tunable wettability fabricated by a green approach, *Mater. Lett.*, 2021, **300**, 130186.

16 B. J. Privett, J. Youn, S. A. Hong, J. Lee, J. Han, J. H. Shin and M. H. Schoenfisch, Antibacterial fluorinated silica colloid superhydrophobic surfaces, *Langmuir*, 2011, **27**, 9597–9601.

17 J. Zhu, C.-M. Hsu, Z. Yu, S. Fan and Y. Cui, Nanodome solar cells with efficient light management and self-cleaning, *Nano Lett.*, 2010, **10**, 1979–1984.

18 L. Zhao, Q. Liu, R. Gao, J. Wang, W. Yang and L. Liu, One-step method for the fabrication of superhydrophobic surface on magnesium alloy and its corrosion protection, antifouling performance, *Corros. Sci.*, 2014, **80**, 177–183.

19 G. Momen and M. Farzaneh, Facile approach in the development of icephobic hierarchically textured coatings as corrosion barrier, *Appl. Surf. Sci.*, 2014, **299**, 41–46.

20 C. R. Crick, J. A. Gibbins and I. P. Parkin, Superhydrophobic polymer-coated copper-mesh; membranes for highly efficient oil–water separation, *J. Mater. Chem. A*, 2013, **1**, 5943–5948.

21 B. Bhushan and Y. C. Jung, Natural and biomimetic artificial surfaces for superhydrophobicity, self-cleaning, low adhesion, and drag reduction, *Prog. Mater. Sci.*, 2011, **56**, 1–108.

22 E. Vazirinasab, R. Jafari and G. Momen, Application of superhydrophobic coatings as a corrosion barrier: a review, *Surf. Coat. Technol.*, 2018, **341**, 40–56.

23 B. Li, J. Bai, J. He, C. Ding, X. Dai, W. Ci, T. Zhu, R. Liao and Y. Yuan, A Review on Superhydrophobic Surface with Anti-Icing Properties in Overhead Transmission Lines, *Coatings*, 2023, **13**, 301.

24 P. Liu, Y. Gao, F. Wang, J. Yang, X. Yu, W. Zhang and L. Yang, Superhydrophobic and self-cleaning behavior of Portland cement with lotus-leaf-like microstructure, *J. Cleaner Prod.*, 2017, **156**, 775–785.

25 A. J. Greer, J. Jacquemin and C. Hardacre, Industrial Applications of Ionic Liquids, *Molecules*, 2020, **25**, 5207.

26 S. L. I. Toh, J. McFarlane, C. Tsouris, D. W. DePaoli, H. Luo and S. Dai, Room-Temperature Ionic Liquids in Liquid–Liquid Extraction: Effects of Solubility in Aqueous Solutions on Surface Properties, *Solvent Extr. Ion Exch.*, 2006, **24**, 33–56.

27 K. S. Khoo, W. Y. Chia, K. Wang, C.-K. Chang, H. Y. Leong, M. N. B. Maaris and P. L. Show, Development of proton-exchange membrane fuel cell with ionic liquid technology, *Sci. Total Environ.*, 2021, **793**, 148705.

28 C. J. Clarke, W.-C. Tu, O. Levers, A. Brohl and J. P. Hallett, Green and sustainable solvents in chemical processes, *Chem. Rev.*, 2018, **118**, 747–800.

29 M. J. Earle, J. M. Esperança, M. A. Gilea, J. N. Canongia Lopes, L. P. Rebelo, J. W. Magee, K. R. Seddon and

J. A. Widegren, The distillation and volatility of ionic liquids, *Nature*, 2006, **439**, 831–834.

30 J. J. Raj, S. Magaret, M. Pranesh, K. C. Lethesh, W. C. Devi and M. I. A. Mutalib, Dual functionalized imidazolium ionic liquids as a green solvent for extractive desulfurization of fuel oil: toxicology and mechanistic studies, *J. Cleaner Prod.*, 2019, **213**, 989–998.

31 A. Bera, in *Green Sustainable Process for Chemical and Environmental Engineering and Science*, ed. D. Inamuddin and T. Altalhi, Elsevier, 2023, pp. 125–144.

32 S. M. H. Sangtarashani, M. Rahmaninia, R. Behrooz and A. Khosravani, Lignocellulosic hydrogel from recycled old corrugated container resources using ionic liquid as a green solvent, *J. Environ. Manage.*, 2020, **270**, 110853.

33 J. R. Lim, L. S. Chua and A. A. Mustaffa, Ionic liquids as green solvent and their applications in bioactive compounds extraction from plants, *Process Biochem.*, 2022, **122**, 292–306.

34 C.-W. Cho, T. P. T. Pham, Y. Zhao, S. Stolte and Y.-S. Yun, Review of the toxic effects of ionic liquids, *Sci. Total Environ.*, 2021, **786**, 147309.

35 H. Mu, X. Peng, J. Chen and F. Zhang, Toxicity of [C8mim]PF6 to aquatic organisms, *China Environ. Sci.*, 2009, **29**, 1196–1201.

36 J. Pernak, I. Goc and I. Mirska, Anti-microbial activities of protic ionic liquids with lactate anion, *Green Chem.*, 2004, **6**, 323–329.

37 J. Ranke, K. Mölter, F. Stock, U. Bottin-Weber, J. Poczobutt, J. Hoffmann, B. Ondruschka, J. Filser and B. Jastorff, Biological effects of imidazolium ionic liquids with varying chain lengths in acute Vibrio fischeri and WST-1 cell viability assays, *Ecotoxicol. Environ. Saf.*, 2004, **58**, 396–404.

38 D. Bains, G. Singh, J. Bhinder, P. K. Agnihotri and N. Singh, Ionic Liquid-Functionalized Multiwalled Carbon Nanotube-Based Hydrophobic Coatings for Robust Antibacterial Applications, *ACS Appl. Bio Mater.*, 2020, **3**, 2092–2103.

39 A. Misra, I. Franco Castillo, D. P. Müller, C. González, S. Eyssautier-Chuine, A. Ziegler, J. M. de la Fuente, S. G. Mitchell and C. Streb, Polyoxometalate-Ionic Liquids (POM-ILs) as Anticorrosion and Antibacterial Coatings for Natural Stones, *Angew. Chem., Int. Ed.*, 2018, **57**, 14926–14931.

40 Q. Ye, T. Gao, F. Wan, B. Yu, X. Pei, F. Zhou and Q. Xue, Grafting poly(ionic liquid) brushes for anti-bacterial and anti-biofouling applications, *J. Mater. Chem.*, 2012, **22**, 13123–13131.

41 I. M. Gindri, K. L. Palmer, D. A. Siddiqui, S. Aghyarian, C. P. Frizzo, M. A. P. Martins and D. C. Rodrigues, Evaluation of mammalian and bacterial cell activity on titanium surface coated with dicationic imidazolium-based ionic liquids, *RSC Adv.*, 2016, **6**, 36475–36483.

42 L. Jin, Z. Shi, X. Zhang, X. Liu, H. Li, J. Wang, F. Liang, W. Zhao and C. Zhao, Intelligent antibacterial surface based on ionic liquid molecular brushes for bacterial killing and release, *J. Mater. Chem. B*, 2019, **7**, 5520–5527.

43 Z. Zheng, Q. Xu, J. Guo, J. Qin, H. Mao, B. Wang and F. Yan, Structure–Antibacterial Activity Relationships of Imidazolium-Type Ionic Liquid Monomers, Poly(ionic liquids) and Poly(ionic liquid) Membranes: Effect of Alkyl Chain Length and Cations, *ACS Appl. Mater. Interfaces*, 2016, **8**, 12684–12692.

44 X. Zhang, M. Cui, L. Nian, P. Wang, Q. Rong, L. Shui, R. Coehoorn, G. Zhou and N. Li, Ionic liquid-modified ZnO-based electron transport layer for inverted organic solar cells, *J. Mater. Sci.: Mater. Electron.*, 2020, **31**, 12678–12683.

45 S. K. Hau, H.-L. Yip, N. S. Baek, J. Zou, K. O'Malley and A. K.-Y. Jen, Air-stable inverted flexible polymer solar cells using zinc oxide nanoparticles as an electron selective layer, *Appl. Phys. Lett.*, 2008, **92**, 253301.

46 S. B. Srivastava, S. K. Srivastava and S. P. Singh, Molecular-Shape-Induced Efficiency Enhancement in PC61BM and PC71BM Based Ternary Blend Organic Solar Cells, *J. Phys. Chem. C*, 2017, **121**, 17104–17111.

47 Y. Zhou, Q. Yao, T. Zhang, X. Chen, Z. Wu, N. Zhang, Y. Shao and Y. Cheng, Antibacterial activity and mechanism of green tea polysaccharide conjugates against Escherichia coli, *Ind. Crops Prod.*, 2020, **152**, 112464.

48 X. Cai, X. Wang, Y. Chen, Y. Wang, D. Song and Q. Gu, A natural biopreservative: Antibacterial action and mechanisms of Chinese Litsea mollis Hemsl. extract against Escherichia coli DH5α and Salmonella spp, *J. Dairy Sci.*, 2019, **102**, 9663–9673.

49 P. Mandal, J. Ivvala, H. S. Arora, S. K. Ghosh and H. S. Grewal, Bioinspired micro/nano structured aluminum with multifaceted applications, *Colloids Surf., B*, 2022, **211**, 112311.

50 P. Mandal, S. K. Ghosh and H. S. Grewal, Graphene oxide coated aluminium as an efficient antibacterial surface, *Environ. Technol. Innovation*, 2022, **28**, 102591.

51 P. Mandal, A. Shishodia, N. Ali, S. Ghosh, H. S. Arora, H. S. Grewal and S. K. Ghosh, Effect of topography and chemical treatment on the hydrophobicity and antibacterial activities of micropatterned aluminium surfaces, *Surf. Topogr.: Metrol. Prop.*, 2020, **8**, 025017.

52 M. J. Hajipour, K. M. Fromm, A. A. Ashkarran, D. J. de Aberasturi, I. R. de Larramendi, T. Rojo, V. Serpooshan, W. J. Parak and M. Mahmoudi, Antibacterial properties of nanoparticles, *Trends Biotechnol.*, 2012, **30**, 499–511.

53 U. N. Maiti, Sk. F. Ahmed, M. K. Mitra and K. K. Chattopadhyay, Novel low temperature synthesis of ZnO nanostructures and its efficient field emission property, *Mater. Res. Bull.*, 2009, **44**, 134–139.

54 R. J. Good, Contact angle, wetting, and adhesion: a critical review, *J. Adhes. Sci. Technol.*, 1992, **6**, 1269–1302.

55 M. E. Schrader, Young-dupre revisited, *Langmuir*, 1995, **11**, 3585–3589.

56 N. W. Robert, Resistance of solid surfaces to wetting by water, *Ind. Eng. Chem.*, 1936, **28**, 988–994.

57 A. Cassie and S. Baxter, Wettability of porous surfaces, *Trans. Faraday Soc.*, 1944, **40**, 546–551.

58 H. Tamura, K. Mita, A. Tanaka and M. Ito, Mechanism of Hydroxylation of Metal Oxide Surfaces, *J. Colloid Interface Sci.*, 2001, **243**, 202–207.

59 P. A. Tran and T. J. Webster, Understanding the wetting properties of nanostructured selenium coatings: the role of nanostructured surface roughness and air-pocket formation, *Int. J. Nanomed.*, 2013, **8**, 2001–2009.

60 V. H. Dalvi and P. J. Rossky, Molecular origins of fluorocarbon hydrophobicity, *Proc. Natl. Acad. Sci. U. S. A.*, 2010, **107**, 13603–13607.

61 J. E. George, V. R. M. Rodrigues, D. Mathur, S. Chidangil and S. D. George, Self-cleaning superhydrophobic surfaces with underwater superaerophobicity, *Mater. Des.*, 2016, **100**, 8–18.

62 S.-E. Jin and H.-E. Jin, Antimicrobial Activity of Zinc Oxide Nano/Microparticles and Their Combinations against Pathogenic Microorganisms for Biomedical Applications: From Physicochemical Characteristics to Pharmacological Aspects, *Nanomaterials*, 2021, **11**, 263.

63 O. Choi, K. K. Deng, N.-J. Kim, L. Ross Jr, R. Y. Surampalli and Z. Hu, The inhibitory effects of silver nanoparticles, silver ions, and silver chloride colloids on microbial growth, *Water Res.*, 2008, **42**, 3066–3074.

64 M. Rai, A. Yadav and A. Gade, Silver nanoparticles as a new generation of antimicrobials, *Biotechnol. Adv.*, 2009, **27**, 76–83.

65 R. Brayner, R. Ferrari-Iliou, N. Brivois, S. Djediat, M. F. Benedetti and F. Fiévet, Toxicological impact studies based on Escherichia coli bacteria in ultrafine ZnO nanoparticles colloidal medium, *Nano Lett.*, 2006, **6**, 866–870.

66 P. K. Stoimenov, R. L. Klinger, G. L. Marchin and K. J. Klabunde, Metal oxide nanoparticles as bactericidal agents, *Langmuir*, 2002, **18**, 6679–6686.

67 N. Padmavathy and R. Vijayaraghavan, Enhanced bioactivity of ZnO nanoparticles—an antimicrobial study, *Sci. Technol. Adv. Mater.*, 2008, **9**, 035004.

68 H. J. Forman and M. Torres, Reactive oxygen species and cell signaling: respiratory burst in macrophage signaling, *Am. J. Respir. Crit. Care Med.*, 2002, **166**, S4–S8.

69 H. Chen, C. Liu, D. Chen, K. Madrid, S. Peng, X. Dong, M. Zhang and Y. Gu, Bacteria-targeting conjugates based on antimicrobial peptide for bacteria diagnosis and therapy, *Mol. Pharmaceutics*, 2015, **12**, 2505–2516.

70 L. Zhang, Y. Jiang, Y. Ding, M. Povey and D. York, Investigation into the antibacterial behaviour of suspensions of ZnO nanoparticles (ZnO nanofluids), *J. Nanopart. Res.*, 2007, **9**, 479–489.

71 K. Kairyte, A. Kadys and Z. Luksiene, Antibacterial and antifungal activity of photoactivated ZnO nanoparticles in suspension, *J. Photochem. Photobiol., B*, 2013, **128**, 78–84.

72 L. S. Reddy, M. M. Nisha, M. Joice and P. Shilpa, Antimicrobial activity of zinc oxide (ZnO) nanoparticle against Klebsiella pneumoniae, *Pharm. Biol.*, 2014, **52**, 1388–1397.

73 M. Arakha, M. Saleem, B. C. Mallick and S. Jha, The effects of interfacial potential on antimicrobial propensity of ZnO nanoparticle, *Sci. Rep.*, 2015, **5**, 1–10.

74 V. K. Sharma, R. A. Yngard and Y. Lin, Silver nanoparticles: green synthesis and their antimicrobial activities, *Adv. Colloid Interface Sci.*, 2009, **145**, 83–96.

75 C.-N. Lok, C.-M. Ho, R. Chen, Q.-Y. He, W.-Y. Yu, H. Sun, P. K.-H. Tam, J.-F. Chiu and C.-M. Che, Proteomic analysis of the mode of antibacterial action of silver nanoparticles, *J. Proteome Res.*, 2006, **5**, 916–924.

76 T. Yasui, T. Yanagida, T. Shimada, K. Otsuka, M. Takeuchi, K. Nagashima, S. Rahong, T. Naito, D. Takeshita, A. Yonese, R. Magofuku, Z. Zhu, N. Kaji, M. Kanai, T. Kawai and Y. Baba, Engineering Nanowire-Mediated Cell Lysis for Microbial Cell Identification, *ACS Nano*, 2019, **13**, 2262–2273.

77 M. Zhang, P. Wang, H. Sun and Z. Wang, Superhydrophobic Surface with Hierarchical Architecture and Bimetallic Composition for Enhanced Antibacterial Activity, *ACS Appl. Mater. Interfaces*, 2014, **6**, 22108–22115.

78 G. Bisht and S. Rayamajhi, ZnO Nanoparticles: A Promising Anticancer Agent, *Nanobiomedicine*, 2016, **3**, 9.

79 A. Ali, A.-R. Phull and M. Zia, Elemental zinc to zinc nanoparticles: is ZnO NPs crucial for life? Synthesis, toxicological, and environmental concerns, *Nanotechnol. Rev.*, 2018, **7**, 413–441.

80 B. D. Rabideau, K. N. West and J. H. Davis, Making good on a promise: ionic liquids with genuinely high degrees of thermal stability, *Chem. Commun.*, 2018, **54**, 5019–5031.

81 K. Fujita, D. Kobayashi, N. Nakamura and H. Ohno, Direct dissolution of wet and saliferous marine microalgae by polar ionic liquids without heating, *Enzyme Microb. Technol.*, 2013, **52**, 199–202.

82 K. M. Docherty and C. F. Kulpa, Jr., Toxicity and antimicrobial activity of imidazolium and pyridinium ionic liquids, *Green Chem.*, 2005, **7**, 185–189.

83 K. Bakshi, S. Mitra, V. K. Sharma, M. S. K. Jayadev, V. G. Sakai, R. Mukhopadhyay, A. Gupta and S. K. Ghosh, Imidazolium-based ionic liquids cause mammalian cell death due to modulated structures and dynamics of cellular membrane, *Biochim. Biophys. Acta, Biomembr.*, 2020, **1862**, 183103.

84 G. Bhattacharya, R. P. Giri, H. Saxena, V. V. Agrawal, A. Gupta, M. K. Mukhopadhyay and S. K. Ghosh, X-ray Reflectivity Study of the Interaction of an Imidazolium-Based Ionic Liquid with a Soft Supported Lipid Membrane, *Langmuir*, 2017, **33**, 1295–1304.

85 S. Mitra, R. Das, A. Singh, M. K. Mukhopadhyay, G. Roy and S. K. Ghosh, Surface Activities of a Lipid Analogue Room-Temperature Ionic Liquid and Its Effects on Phospholipid Membrane, *Langmuir*, 2020, **36**, 328–339.